Astrocytes are active: An information theoretic approach reveals differences in Ca2+ signaling patterns among distinct astrocyte subtypes

Authors:

Nicholas J. Mennona[1,2], Barbara Barile[3], Hoony Kang[1,2], Valentina Benfenati[4], Grazia P. Nicchia[3], Kate M. O'Neill [1], Wolfgang Losert [1,2]

1 Institute for Physical Sciences & Technology, Univ. of Maryland, Col. Park, College Park, MD, USA
2 Physics Dept., Univ. of Maryland, Col. Park, College Park, MD, USA
3 Biosciences, Biotechnology and Environment, University of Bari Aldo Moro, 70125, Bari, Italy
4 Institute of Organic Synthesis and Photoreactivity, National Research Council of Italy, 40129, Bologna, Italy

Keywords: Collective Dynamics, Information Theory, Astrocytes

Abstract:

The discovery that astrocytes are an active, rather than a passive, component of the brain has ushered in a paradigm shift in thinking about how the brain processes information. Although the mechanisms by which astrocytes integrate information from neurons are still debated, such discourse should not distract from the importance of more completely understanding how astrocytes communicate via signals amongst themselves. This work aims to study how different astrocytes signal within their own networks. We investigate group calcium (Ca^{2+}) dynamics in polygonal, stellate, and reactive astrocytes. These distinct and important astrocyte subtypes are present in the brain to varying degrees at different physiological states. We use an information-theoretic framework to quantify the dynamics embedded in the Ca2+ traces within astrocyte networks; specifically, we employ the Hurst exponent, cross-correlation, mutual information, and partitioned entropy to assess differences in the astrocyte signals across subtypes. To gain insights into the ability of astrocyte networks to respond to changes in the extracellular environment, we probe the networks with perturbations affecting their cytoskeletal dynamics (Latrunculin B) and energetic levels (Adenosine triphosphate). Overall, these three classes of astrocytes behave differently and respond idiosyncratically to their extracellular environment. We find that polygonal astrocytes are not quiescent, stellate astrocytes respond most strongly to ATP, and reactive astrocytes are uniquely perturbed by Latrunculin B. Interestingly, despite these distinct differences in behaviors, we find a uniform speed of information transport regardless of subtype or perturbation; this uniformity is maintained when using both cross-correlation and mutual information to assess this speed. We conclude that the differential ways astrocytes signal within our measured framework yield important insights into how astrocytes communicate and contribute to this pressing issue of understanding astrocyte information processing.

Introduction:

Astrocytes are the most numerous glial cell type in the brain. They are important for physiological functions, including K^+ clearance[1], glutamate homeostasis[2], and extracellular volume regulation[3] (reviewed in[4–6]). Since astrocytes carry out these known supporting functions and lack electrical

excitability, most studies have overlooked the potential active role of astrocytes in information processing. In contrast, neuronal dynamics has become synonymous with information processing[7–12].

Nevertheless, recent work has provided strong indications that astrocytes do play an active role in information processing. As a counterpart to neurons, astrocytes also form their own networks, linked together via gap junctions composed of connexins, including Cx43, one of the main connexins in astrocytes[13,14]. Within these networks, astrocytes signal to each other also via slow Ca^{2+} waves.[15]. Intracellularly, IP_3triggers intercellular Ca^{2+} waves[15] which propagate through astrocyte networks via the aforementioned gap junctions. Recent studies reveal that these waves can occur spontaneously, with excitable dynamics similar to action potentials, although on a slower timescale of seconds[16]. Thus, astrocytes can have an active role in information flow, with calcium waves functioning as non-electrical communication signals. In single astrocytes, these calcium waves are heterogeneous[17] and flow through astrocyte processes and microdomains[18–20]. Methods such as the machine learning tool AQUA now enable robust intracellular analysis of astrocyte calcium[17] for *ex-vivo* and *in vivo* analysis of astrocyte activity.

Calcium signals, occurring either locally in microdomains or spreading into calcium waves also determine the release of bioactive molecules called gliotransmitters from astrocytes. Astrocyte gliotransmission (by e.g. ATP, Glutamate and GABA) is the known information transfer mechanism from astrocytes to neurons, and has been modeled for its role in synaptic plasticity, memory, and learning[21,26–28]. We propose that, to encompass such network scale information, astrocytes should also process and integrate information among themselves.

To support our hypothesis and gain insight on the information flowing between astrocytes and the unexplored network scale implications of that[16], in this work, we utilize physics-based information-theoretic techniques to analyze and describe the behavior of calcium dynamics or pure primary rat culture of astrocytes *in vitro*. The current study contrasts three physiologically relevant subtypes of astrocytes, focusing on their collective (ensemble) dynamics within *in vitro* networks. These *in vitro* cultures remain a powerful tool[16] for analyzing astrocyte dynamics, especially since the current study focuses on how individual astrocytes contribute to the ensemble.

Following established protocols, we study *in vitro* models of polygonal (immature), stellate (healthy), and reactive (immature) astrocytes. Intracellular and extracellular ionic changes are reported to occur upon several physiological and pathophysiological events, including regulation of the activity of chemical synapses, glial scarring[21], synapsis plasticity[22], and formation upon neurodevelopment[23]. Anisosmotic challenges are counterbalanced by water flows, which are predominantly mediated by the water channel aquaporin-4 (AQP4) in brain astrocytes[24]. AQP4 is reported to be polarized and enriched in astrocyte endfeet where it plays a key homeostatic role. By modulating water influx/efflux, it ensures a fine regulation of astrocyte cell volume and morphology, thus preserving brain integrity and functionality[24]. In this view, it is not surprising that AQP4 is found to be co-expressed or functionally coupled in astrocyte membranes with ion channels, including potassium (i.e. Kir4.1[25]) and calcium (i.e. TRPV4) channels[3,24,26]. On the other hand, connexins are shown to take part in astrocytes' response to injury upon the stimulation of pro-inflammatory cytokines, including TGF-beta[27]. An increase in the levels of Cx43 in reactive astrocytes is proposed to act as a supporting mechanism that helps maintain astrocytes' gliotic phenotype and maximize the coordinated intervention of these cells and their communication for the injury resolution[28,29].

The astrocyte networks – polygonal, stellate, and reactive – are broadly classified as immature, healthy, and injured, respectively, and have distinct physiological behavioral profiles[19,30–33]. A key readout of these distinct subtypes is their unique and stark morphologies. The differing structures and morphologies of astrocytes, in general, have been implicated in brain functionality[30,34,35] and the cell-cell signaling of

astrocyte networks[36]. Notably, previous works evidence that different morphologies are paralleled by different functions in astrocytes, such as alteration in the cell volume mechanism[37–39], electrophysiological properties linked with potassium spatial buffering[39,40], and actin dynamics[41]. However, studies are lacking the capability of correlating spatially and temporally the calcium signaling in astrocytes, which are critically implicated in all the above-mentioned astrocytes functions.

With the goal of broadening our understanding of astrocyte-specific calcium signaling, we quantify the collective calcium dynamics, both spontaneous and perturbed, of these astrocytes. We perturb these dynamics *in vitro* cultures with low-dose Latrunculin B (LATB) and Adenosine triphosphate (ATP) as these represent basic perturbations to the cellular cytoskeleton[42–44], and cellular energy[45–48], respectively. Due to the slow and heterogeneous characteristics of astrocyte calcium signaling, astrocyte signals are more analog than digital. Neuronal signals are often treated as digital, 1 (firing) or 0 (not firing). Astrocyte signaling is too slow for such binarization. Thus, information-theoretic methods that extract information without digitizing the signal are used. We employ amplitude ordering symbolization with an embedding window large enough to encapsulate the dynamics of astrocyte calcium events, which are mostly on the order of 1-5.5 seconds[16]. Amplitude ordering, rather than binarizing via the mean, is more appropriate for quantifying the dynamic properties of these nonlinear signals. This nonlinearity allows us to elucidate information characteristics and information speeds across polygonal, stellate, and reactive astrocytes in a comprehensive manner.

Methods

Imaging

Primary astrocytes were obtained from Sprague Dawley rats housed at the University of Maryland (in concordance with the recommendations of and approval by the University of Maryland Institutional Animal Care and Use Committee; protocols R-FEB-21-04). Experiments were performed between 14 to 21 (DIV14-DIV21) days after dissection[49]. At this time, astrocytes were trypsinized from flasks and plated into PDL-coated (Sigma-Aldrich) 35 mm dishes (MatTek). Dishes containing cultured astrocytes were incubated with 5µM CalBryte 590 AM (AAT Bioquest) for 30-60 min at 37°C prior to imaging. Dishes were then washed with PBS. Astrocytes are plated at densities such that they proliferate to roughly 500k cells/well on the day of imaging (a final density of approximately 10k cells/mm^2), and imaging was performed on a spinning disk confocal microscope (PerkinElmer). Image acquisition occurred for approximately 15 minutes at roughly one frame per second with 100 ms of exposure time per frame. The University of Maryland Imaging Core maintains the PerkinElmer spinning disk confocal microscope used for this research. The image sequences were taken by the equipped Hamamatsu ImagEM X2 EM-CCD camera (C9100-23B), which records 16-bit images. Sequences were taken from an air 20x objective (0.75 NA; 0.717 µm per pixel) and under temperature (37°C), CO2 (5%), and humidity control.

All experiments are performed in NeuroBasal media (Gibco). We use this media to simulate a neuronal environment, and we found that it allows for spontaneous activity in unperturbed wells (over DMEM). For simplicity, throughout this manuscript, this environment is referred to as spontaneous (control). ATP (Sigma-Aldrich) and Latrunculin B (Sigma-Aldrich) were applied immediately upon imaging and at low-dose concentrations of 1.5uM for ATP and 0.5uM for Latrunculin B. Unlike Latrunculin A, the slower depolymerization rate of Latrunculin B allows for perturbation of actin without drastically dissociating the entire astrocyte network. The value of Latrunculin was found based on testing whether our astrocyte networks were maintained (expressed minimal disassociation) for the 15-minute duration at the chosen

130 imaging setting (e.g., laser intensity). For simplicity, throughout the rest of this work, we refer to
131 Latrunculin B as LATB.

132 *Cell Culture*

133 Primary astrocytes were obtained from Sprague Dawley rats housed at the University of Maryland (in
134 concordance with the recommendations of and approval by the University of Maryland Institutional
135 Animal Care and Use Committee; protocols R-FEB-21-04). Astrocytes were prepared from 0-to-2 day
136 postnatal (P0-P2) Sprague Dawley rat brains as described previously[41]. Briefly, cortical tissue from each
137 pup was separately dissociated via trituration, filtered, and plated into T25 flasks containing DMEM
138 (ThermoFisher), 15% fetal bovine serum (Benchmark), and 1% penicillin-streptomycin (P/S). After
139 roughly seven days, in order to generate stellate and reactive astrocytes, the media was changed to either
140 (1) stellate media, which includes Neurobasal (ThermoFisher), 2% B27+ (GIBCO), 5 ng/mL HB-EGF
141 (TOCRIS BioSciences)[19] or (2) reactive media, which is serum-free DMEM to which 10 ug/mL of TGF-
142 B1 was added after five additional days *in vitro*[50].

143

144 *Cell lysis and Western Blot*

145 Protein samples were obtained as previously described, with some slight changes[3]. Briefly, astrocytes
146 grown for seven days in control, stellate, and reactive media were washed in ice-cold phosphate-buffered
147 saline (PBS) and scraped with 300 µL of RIPA lysis buffer (10 mM Tris-HCl, pH 7.4, 140 mM NaCl, 1%
148 Triton X-100, 1% Na deoxycholate, 0.1% SDS, 1mM Na3VO4, 1 mM NaF, 1 mM EDTA and 1× Protease
149 Inhibitor Cocktail). Lysates were vortexed every 5 minutes for 30 minutes and centrifuged at 22 000 for 30
150 minutes at 4°C. Supernatants were collected and Pierce™ BCA Protein Assay Kit was used to dose the
151 protein content. 5 µg of proteins/lane were dissolved in Laemmli Sample Buffer (Bio-Rad, Hercules,
152 California, USA) added with 50 mM dithiothreitol, heated to 37°C for 10 min and resolved by SDS-PAGE
153 in 10% (for Cx43 detection) and 12% (for AQP4 and GFAP detection) gels prepared with Mini-PROTEAN
154 TGX Stain-Free Precast polyacrylamide solutions (Bio-Rad, Hercules, California, USA). gels were then
155 activated for 5 minutes on a Chemidoc imaging system (Bio-Rad, Hercules, California, USA) and
156 transferred to polyvinylidene fluoride (PVDF) membranes (Merck Millipore, Burlington, Massachusetts,
157 USA). Stain-free signal of transferred blots was collected. Membranes were incubated with blocking
158 solution and incubated overnight with primary antibodies, rinsed, then incubated with the appropriate
159 peroxidase-conjugated IgG secondary antibodies. Protein-specific bands were revealed using enhanced
160 chemiluminescent Clarity Western ECL Substrate (Bio-Rad, Hercules, California, USA) and visualized on
161 a Chemidoc imaging system. The densitometric analysis was performed in Image Lab software 6.1.0 by
162 normalizing the bands to the stain-free blot signal. The Western blot analysis of Cx43, AQP4, and GFAP
163 for the polygonal, stellate, and reactive astrocytes confirms three distinct phenotypes: reactive upregulate
164 Cx43 and AQP4, stellate upregulate AQP4, and polygonal cells do not express any of these markers
165 significantly.

166

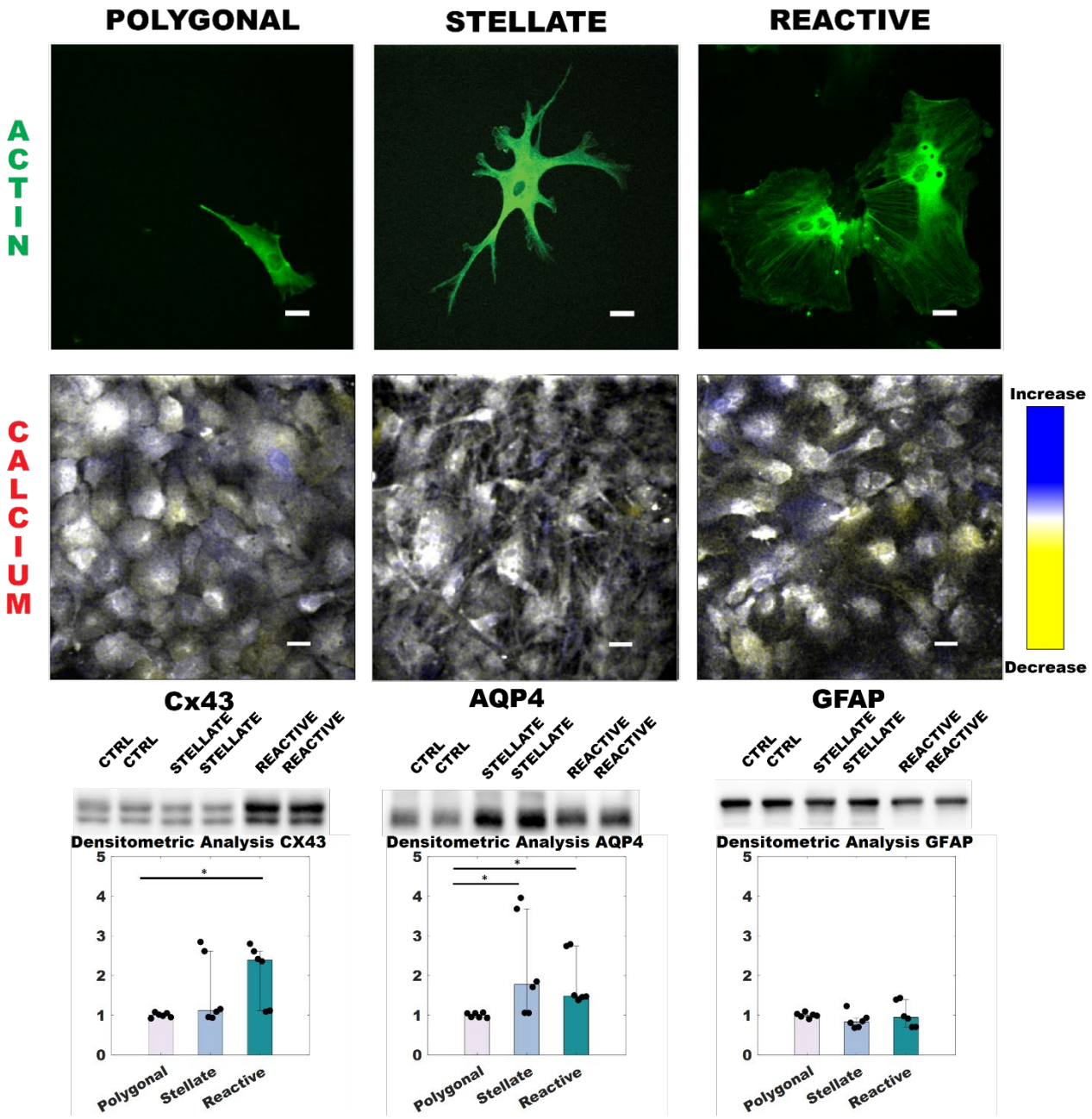

*Fig 1: Astrocyte morphologies (polygonal, stellate, and reactive). The phenotypes correspond to different morphologies, as shown in green via actin images. Images of actin are acquired with 488nm light of astrocytes that express BacMam Actin-GFP. We record the calcium signaling channels of these dense astrocyte networks with 561 nm light of astrocyte networks stained with CalBryte 590. It has been noted that, regardless of protocol, different media formulations result in different morphologies for astrocytes[19]. We use time overlays to show the different manifestations of calcium propagation in the distinct morphological conditions of astrocytes. Blue corresponds to an increase in [$Ca2^{+}$] during this frame, yellow a decrease, and white means that this frame contains values similar to the previous timepoint. Western Blot analysis of Cx43, AQP4, and GFAP in polygonal, stellate, and reactive astrocytes. The upper panels show Cx43 (band at ~43kDa), AQP4 (band at ~30-32 kDa), and GFAP expression (band at ~50 kDa) in primary rat astrocytes. Western Blot analysis of Cx43, AQP4, and GFAP in polygonal, reactive, and stellate astrocytes. Western Blot showing Cx43 (band at ~43 kDa), AQP4 (band at ~30-32 kDa), and GFAP expression (band at ~50 kDa) in rat astrocytes. Using Kruskal Wallis Dunn's multiple comparison test, we find statistical significance for polygonal compared to stellate (AQP4) and reactive (Cx43 and AQP4). *p< 0.05; **p<0.01. Scale bars are 25 µm.*

181 In this work, we investigate astrocytes of three physiological types; a prominent distinguishing
182 characteristic of the differences is seen in the differences in morphology. Fig. 1 (top) provides representative
183 images of the three classes of astrocytes analyzed in this study. Each astrocyte network does not contain a
184 mix of different cell types and is cultured to maintain a singular physiological expression. For these
185 astrocyte types, we investigate collective Ca2+ dynamics as illustrated in Fig 1 (middle), where multiple
186 frames are overlaid to demonstrate the distribution of Ca^{2+} fluctuations (rising calcium in blue, diminishing
187 calcium in yellow) in a network. Through Western blot analysis, we evaluated the expression profiles of 1)
188 Cx43, one of the major isoforms forming astrocytic gap-junctions involved in calcium-mediated cell-to-
189 cell communication, as a molecular marker of intercellular connectivity within astrocytes networks; 2)
190 AQP4, the most abundantly expressed water channel in brain astrocytes, and GFAP, the predominant
191 intermediate filament of the astrocyte cytoskeleton in the CNS, as proxy markers of cell differentiation and
192 reactivity[3,51,52].

193 AQP4 and its supramolecular level of organization in larger-sized assemblies have been reported to
194 correlate with the morphological and functional maturity of astrocytes in CNS postnatal development[53] as
195 well as in in-vitro models of astrocyte differentiation[3]. Therefore, the overexpression of AQP4 in stellate
196 astrocytes is likely to refer to the morphological differentiation of this cell type in the experimental
197 conditions. The overexpression of Cx43 in the reactive conditions might be ascribable to the acquisition in
198 vitro of the in vivo-like reactive state that makes astrocytes more prompt at tissue healing and wound repair.

199 As for GFAP, besides the number of studies that identified a positive role for these canonical hallmarks of
200 astrogliosis, just as many provided opposite evidence. On one hand, it was previously found to be
201 downregulated in similar or even different models of astrogliosis (i.e., TNF and IL-1β[54–56] and LPS-treated
202 astrocytes[57]. On the other hand, its upregulation was associated with beneficial and neuroprotective effects
203 i.e., enhancing neuronal regeneration through protein re-localization, increasing the membrane retention of
204 glutamate transport GLAST in astrocytes, which protects surrounding neurons from glutamate
205 excitotoxicity[58]; providing scaffolds for new neurites[59]. In the present study, no changes were detected in
206 the three conditions, although we could detect differences in other markers in response to inflammatory
207 (i.e., Cx43) and differentiation stimuli (i.e., AQP4; Cx43). We, therefore, anticipate that GFAP might not
208 be a reliable marker to assess astrocytes' degree of astrogliosis or differentiation.

209 Western blot analysis shows that the three cell types have distinct expression profiles of the aforementioned
210 astrocyte proteins. Of note, we found that Cx43 is upregulated in the reactive state compared to control and
211 stellate astrocytes (Fig.1, bottom left panel), while AQP4 is overexpressed both upon stimulation with TGF-
212 beta and in star-shaped astrocytes, differently from controls (Fig.2, bottom middle panel). GFAP was
213 equally abundant in the three conditions with no statistical significance (Fig.1, bottom right panel).

214 Overall, while illustrating that the proteins undergo distinct changes in their profile expression in response
215 to the different external stimuli provided under culture conditions, these results also provide evidence that
216 the three cell types can be regarded as distinct "phenotypes" from the molecular perspective.

217

218 *Analytical Methods*

219 To analyze the calcium dynamics of astrocytes, we first segment individual astrocyte objects within our
220 imaging datasets using the morphological watershed algorithm FogBank[60]. Manually, we refined
221 parameters per each imaging sequence such that segmented boundaries roughly correspond to the
222 distinctions made by eye. FogBank preserves the unique heterogeneity of astrocyte bodies rather than
223 using the cell center with an arbitrary radius, as is typically done with neuron-imaging analysis[61]. See
224 Supplement for a representative FogBank example. All image sequences are jitter corrected, and Gaussian
225 smoothed in the spatial domain before further analysis. For each frame in a dataset, we take the median
226 fluorescence value from all the pixels identified within the astrocyte object, as shown in the five objects in

Fig 2A. We compute relative fluorescence measure ($\Delta F/F_0$), where $\Delta F=F-F_0$, for each astrocyte object. F_0 is computed using a window of approximately 30s (30 frames, 15 back, 15 forward) where F_0 is the average of the fluorescence values below the 50th percentile of values contained within the window[62]. This is called a trace. Throughout the paper, for convenience, we address this fluorescence measure as DF/F. As seen in representative traces, peaks in calcium dynamics are broad and not well-defined. The sliding window is chosen based on an inspection of the data and does not meaningfully change the dynamic properties of the traces. Please consult the Supplement for more details. We chose this window size based on experimental observation of astrocyte calcium event duration. Examples of such traces are shown in Fig 2B. Recall that astrocytes are not neurons, so it is inappropriate to call the activity of our traces 'spikes.' Instead, we use the term "calcium event" to describe the smooth rises and falls exhibited by traces in Fig 2B.

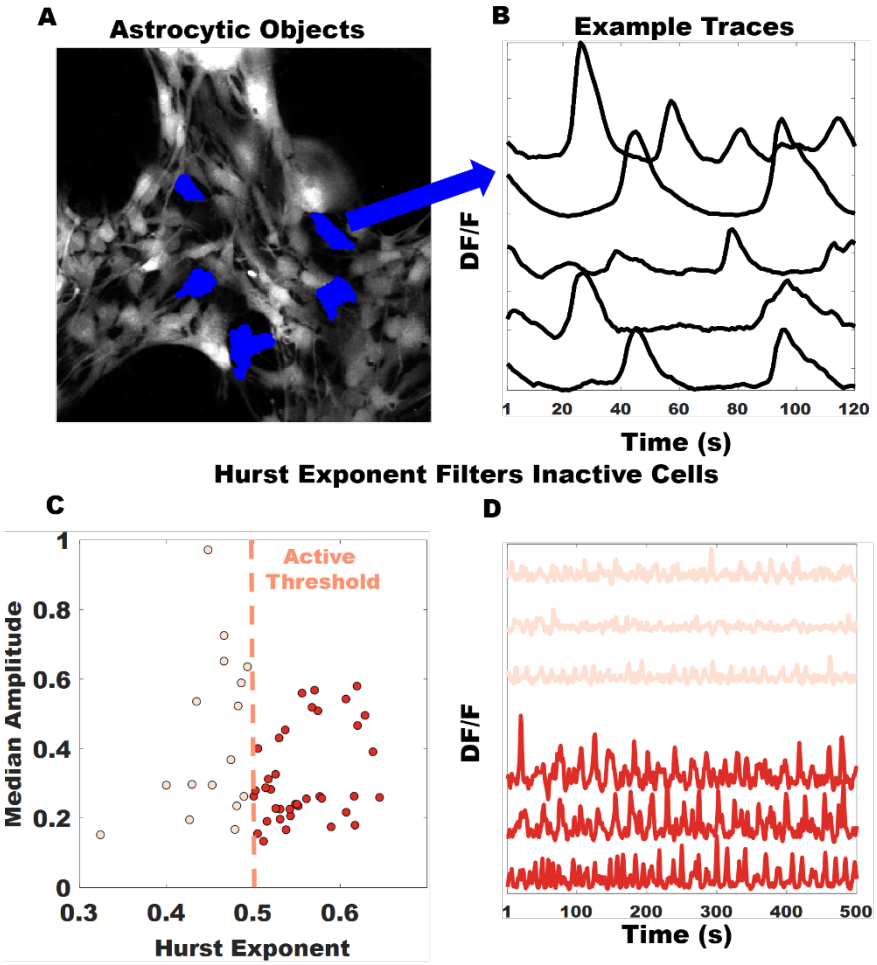

Fig 2: Astrocytes traces extracted and filtered using Hurst exponent. (A) Given a dense astrocytic network, astrocytic elements are segmented using FogBank. Examples of astrocytic elements extracted. (B) DF/F traces of the five objects extracted in blue (dark pixelated objects) are shown. (C) Hurst exponent measures memory in a time series, which is used to filter out inactive cells or poorly segmented objects. Inactive (salmon, light) versus active (red, dark) cells plotted. Only time series with Hurst exponents greater than or equal to 0.5 are used. (D) From the example points, we plot representative inactive and active traces.

Our goal is to use traces that show persistent calcium signals and to distinguish them from random fluctuations of signals in the networks. Our goal is to define traces that exhibit smooth and meaningful

247 rises and falls (see red, darker curves in Fig 2D) as 'active,' regardless of the intensity values. The Hurst
248 Exponent (defined as *H*) allows us to carry out this analysis. H is defined for a given time series x(t) as:

249 $$< |x(t+\tau) - x(t)|^2 > \sim \tau^{2H}$$

250 *Equation 1*

251 We find that the Hurst exponent provides a robust and reliable way of filtering out noisy traces due to
252 poor segmentation or weak calcium signals. Hurst exponent values below a threshold of 0.5 represent
253 random activity, and the corresponding traces (e.g., the salmon, lighter colored curves in Fig 2D) are
254 excluded from the analysis[63,64].

255 The importance of correlations in neuronal encoding is well-cited in the literature[65–68].The study of
256 correlation in the brain relates to the collective activity of neuronal ensembles in relation to information
257 encoding and processing in the brain. This level of mathematical rigor has not been applied to astrocyte-
258 only networks, and the study of correlation within astrocyte networks has only been viewed in the context
259 of neuronal activation[69]. Given the success of using these methods on neurons and the absence of their use
260 in analyzing astrocytes, we argue that our use of these methods should yield comparable success and
261 insight. Correlations allow us to understand the global characteristics of an ensemble of active nodes (in
262 this case, astrocytes). However, we can alternatively view the dynamics in our astrocyte networks as a
263 dynamical system that is affected by individual astrocytes, i.e., the local dynamics of one trace affecting
264 the global dynamics observed. Since our Western blot analysis confirms cell-cell coupling, we argue that
265 these readouts provide a fairly accurate representation of the information processing performed by these
266 collections of astrocytes. This approach has been well-documented experimentally (e.g., with neuronal
267 MRI data) and theoretically[70–78] . A limitation of correlations is that the global characteristics of a network
268 are studied by assessing each cell's connections to others in the network. Information theory helps
269 overcome such limitations. An information theoretic approach can analyze a network for each astrocyte
270 rather than for pairs of cells. Thus, this approach provides a robust metric for assessing each individual
271 astrocyte's contribution to the mean field or the group characteristics of the network.

272 To implement this approach, from the extracted traces, we convert the traces into states using
273 symbolization[70,79]. This symbolization enables the interpretation of changes in calcium as an analog
274 signal; traces that exhibit lower entropy correspond to traces with more periodic fluctuations. We take the
275 time traces shown in Fig 3A, the amplitude order of each timepoint in a window, and convert this set of
276 timepoints into a state (an example suite of states is available in Fig 3B), and then convert the traces into
277 symbol sequences visualized in Fig 3C. As an illustrative example with a manageable number of states,
278 m=3 has been used (number of states = m!). From the resulting symbol sequence, we can find the
279 probability distributions of states (Fig 3D). The probability of states, in turn, allows us to compute an
280 information entropy for this representation of calcium traces. Amplitude ordering entails choosing two
281 parameters, m, and l, where m defines the embedding dimension[70,78] (the symbol set size that functions as
282 a coarse-graining window) and l denotes the time lag[78]. A more comprehensive review of this
283 symbolization method can be found in Refs[70–72,74,76–79]. We choose m to smooth out noise without losing
284 actual spikes in the data. Based on our experimental observation of the duration of calcium events in our
285 data, we chose m=5 and l=1. As m takes the role of the coarse-graining window, l can be kept at its
286 minimum (l=1) to prevent further information down-sampling.

287 Given that we have converted these time series into symbol series, we can perform time-delayed mutual
288 information methods. Time-delayed mutual information is the symbolized equivalent of cross-correlation.
289 Moreover, given that astrocyte signals are nonlinear, mutual information is a more appropriate method
290 than Granger causality[80]. While there are some similarities between mutual information and cross-
291 correlation, we emphasize that mutual information discusses the dynamics of symbols (with embedded

dynamics) from a probability distribution. Cross-correlation looks at the absolute fluctuations from the mean for traces. In some regards, then, symbolization can be viewed as the differential expression of trace dynamics. Lastly, from both of these measures, we can quantify the speed of information transport[81]. We can measure speed from the measured distances between astrocytes and either the cross-correlation time lag or the time lag associated with the mutual information measurement.

Additionally, we analyze the information content of astrocyte networks with partitioned entropy. Partitioned entropy $h_a(\tau)$ is a useful metric for understanding the time-evolution of states over a certain

$$h_a(\tau) = -\sum_{i=1}^{m!} p_{ai}(\tau) \ln\, p_{ai}(\tau)$$

Equation 2

where $p_{ai}(\tau)$ represents the probability that the system evolves from state a to state i at τ timesteps. Partitioned entropy differs from canonical entropy as it is a function of time. We employ this approach to understand better how the ramps and falls of these calcium fluctuations evolve differentially for all of the cells within the unique networks. A schematic for understanding partitioned entropy is shown in Fig 3E. We validated this analysis on both regular and chaotic time series data.[72] See Supplement for details. As a clarification, we note that the symbolization described enables analysis of

Shannon entropy. The rest of the analysis refers to Shannon entropy and the dynamics therein, e.g., partitioned (Shannon) entropy.

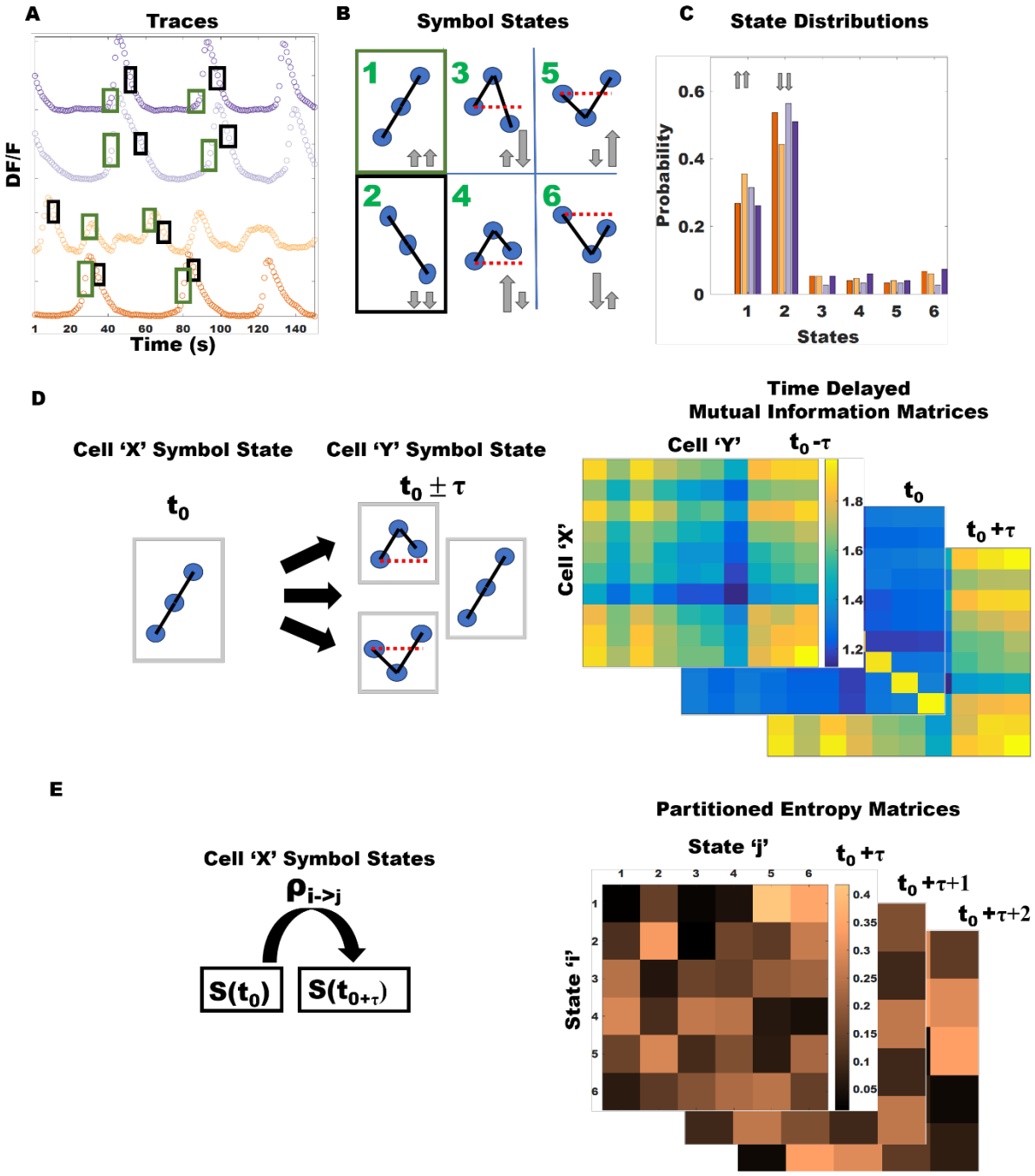

Fig. 3: Methods for Information Theoretic Approach to Collective Astrocyte Dynamics. (A) Astrocyte traces. Different shaded boxes correspond to example symbol states. (B) Symbol states. Shaded boxes are those previously overlaid on traces. In this figure, have used an m of 3 as this corresponds to 6 possible states for every time window (m!=6). We note, using grey arrows, the physical dynamics behind each state (for states 1 and 2, the same size for the arrows is for visual purposes). (C) Symbol sequences for the traces shown previously. (D) Visualization of Time-Delayed Mutual Information. (E) Example subset of transition probabilities from states to future states for some given tau for any particular state 'i'. See Equation 1 for more details. This subfigure represents partitioned entropy.

Results

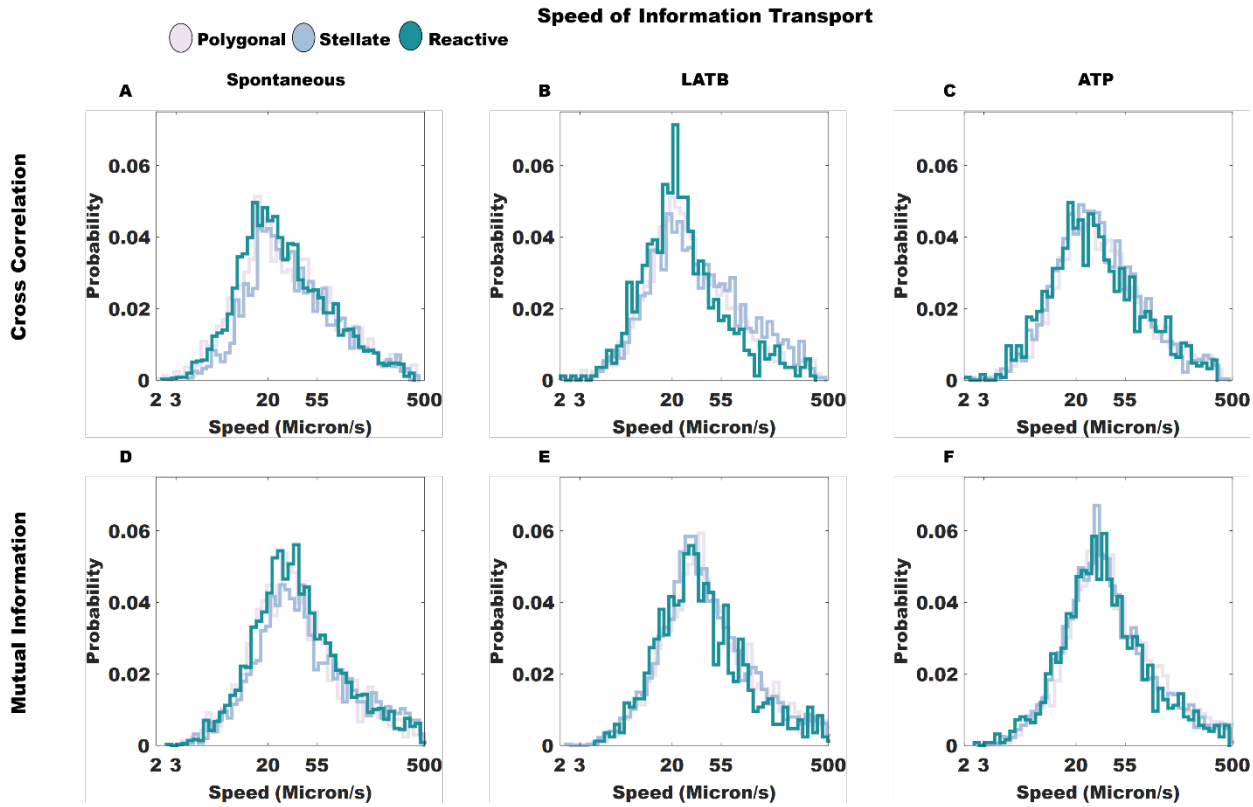

Fig 4: Speeds of Information Transport via Cross Correlation and Mutual Information. Figures shown for all distinct subtypes of astrocyte. Cross correlation speeds are shown for (A) spontaneous, (B) ATP, and (C) LATB affected networks. Mutual information speeds are displayed for (D) spontaneous, (E) ATP, and (F) LATB affected networks. Due to the skewed nature of all distributions, these distributions have been log-normalized. We find the speed of information transport is invariant across astrocyte subtype and extracellular environment.

Astrocyte Speed of Information Transport

An important metric for assessing how astrocyte transport information is information speed (speed of information transport). This ad-hoc (average) metric is extracted for free by any time lag calculation. We do not track calcium flow, but can track the exchange of information as a function of time and distance between cells. This method has been used for mutual information[81]; we extend it for cross correlation since the time lag associated with maximal cross correlation is similarly extracted. Our measure of speed is average ($v = DIST/\tau$), it coarsely reveals the rate at which these pairwise quantities are absolutely maximized, reflecting the nature of the timescales associated with astrocyte calcium events. Additionally, the maximal time lags found are rate-limited by the acquisition speed, which is 1 Hz. Due to the 1 Hz frame rate and other coarse graining involved (e.g. distance is computed from center of mass points in a segmented image), this measure is an average metric. Thus, we conclude that a few micron per second difference is not significant to ascertain any meaningful discrepancy from a biological perspective.

We describe the cross-correlation speeds first. The distributions are modelled as a lognormal distribution to obtain the mean speeds to follow as shown in Figs 4A-C. Outliers at infinity are removed (which may happen for time lags of zero). We report the mean of these distributions modeled under lognormal

assumptions. The spontaneous speeds are: for polygonal 25 μm/s, for stellate 28 μm/s, for reactive 23 μm/s. Under LATB, for polygonal 25 μm/s, for stellate 27 μm/s, for reactive 21 μm/s. With ATP, for polygonal, 29 μm/s, for stellate 28 μm/s, for reactive 25 μm/s. As expressed in Figs 4A-C, these distributions are not symmetric (not entirely lognormal). Given that the order of difference between stellate and other networks is ~5 μm/s at most, and the distributions themselves retain similar characteristics (the distributions peak within this 20-30 μm/s range consistent with experimental studies), we conclude that the speed of information transport is invariant across astrocyte subtypes and conditions.

Next, we report the mutual information speeds. The spontaneous speeds are: for polygonal 28 μm/s, for stellate 32 μm/s, for reactive 30 μm/s. Under LATB, for polygonal 34 μm/s, for stellate 32 μm/s, for reactive 29 μm/s. With ATP, for polygonal 34 μm/s, stellate 30 μm/s, and reactive 29 μm/s. These mean values are reported from modelling the distributions as lognormal. We conclude that the apparent differences between the reported mean values are minimized for mutual information speeds. The speeds are slightly higher than those of cross correlation. All speeds are in the ~30-35 μm/s. This range is roughly consistent with the cross-correlation speeds (at the higher end), and is consistent with the reported literature.

Largely, we find a constant speed of information transport across conditions and types. Using this metric (defined as distance between objects divided by the time lag associated with maximization of pairwise quantity), we find that all distributions sharply peak similarly within the reported experimental range for calcium wave speeds. The nature of these distributions across both subtype and conditions suggests an invariance of the speed of information transport in astrocyte networks using this coarse approximation. The similarities in the relationships between the distributions for the quantities (mutual information and cross-correlation are similar, but differently formulated) reflects that the aggregate relationships between calcium signals for astrocytes are independent of subtype and perturbation. This counter-intuitive result suggests that astrocytes regulate ions' flow despite cellular state, and maintain homeostasis in stressful environments to maintain signaling speeds.

As a final remark, we comment that the time-lags associated with either maximal cross-correlation or mutual information may come from a symmetric peaking in a time-lag curve (i.e. bimodal peaks about the y-axis). We argue that many of the time lags reflect a maximal value over a relevant physiological window. All other lags reflect a mode within the time-lag curves themselves. This argument is expanded in the Supplement.

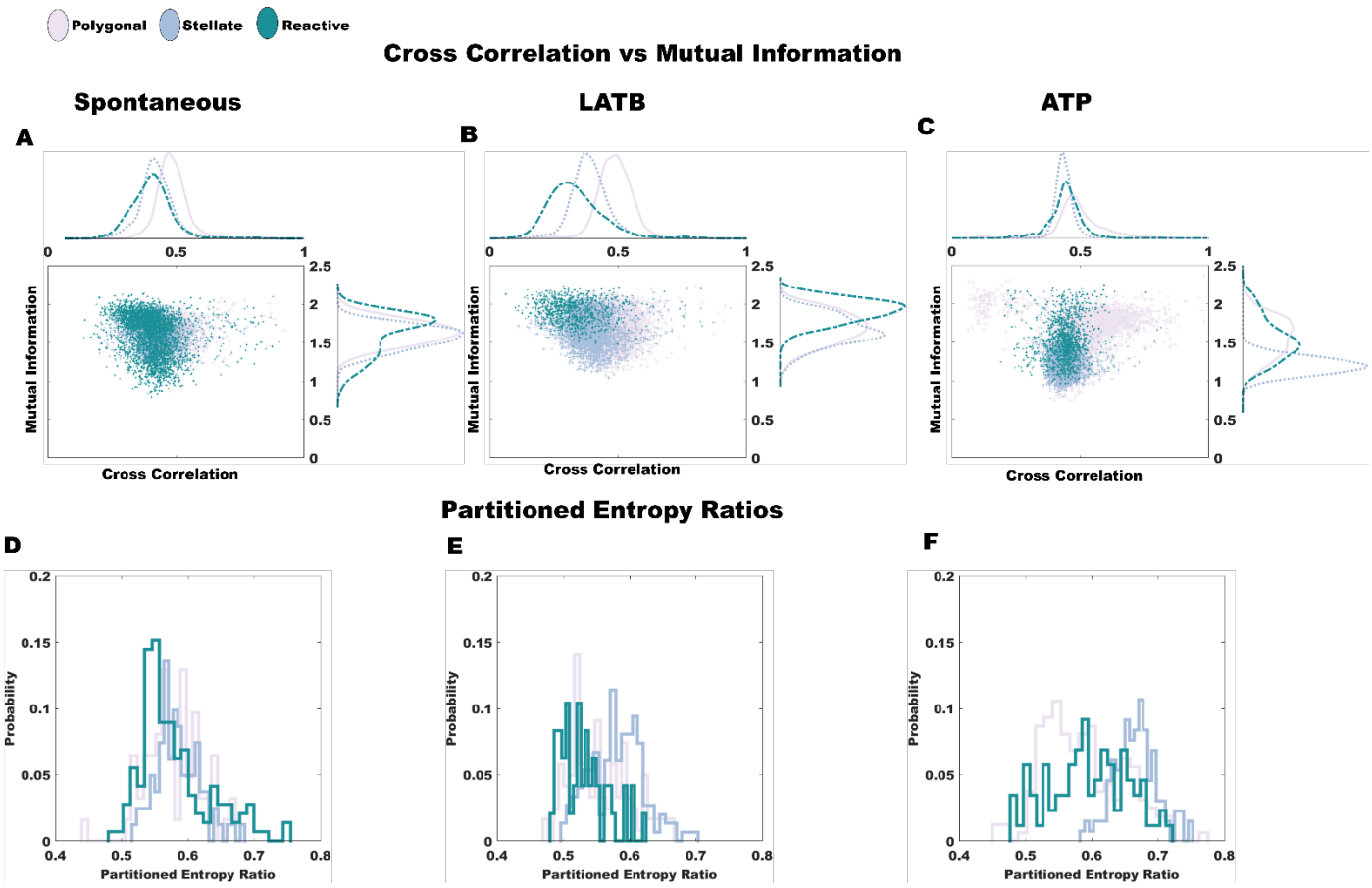

Fig 5: Cross correlation versus mutual information, and partitioned entropy comparisons. We compare the distributions of both maximal cross correlation and maximal mutual information across time for (A) spontaneous, (B) LATB-induced, and (C) ATP-enhanced astrocyte networks. Each point represents the cross correlation (x-axis) and mutual information (y-axis) for the same pair of cells. We then look at the dynamics of individual traces using partitioned entropy for (D) spontaneous, (E) LATB-induced, and (F) ATP-enhanced networks. Partitioned entropy ratio is the average of the partitioned entropy divided by the entropy.

Information exchange of signaling amongst active astrocytes

Next, we assess how the traces in astrocyte networks can be used to infer relationships across pairs of cells. Given a time window of 31 frames (roughly 31 s), we find the maximum cross correlation and mutual information values. These relationships are shown in Figs 5A-C. First, we discuss the cross-correlation distributions. In spontaneous conditions, polygonal astrocyte pairs have higher cross correlation subtype, but stellate and reactive pairs demonstrate comparable distributions (Fig 5A). When LATB is introduced into the astrocyte networks; the distributions are separable indicating that the breakdown of the actin cytoskeleton causes idiosyncratic (i.e. each astrocyte network varies its distribution relative to its spontaneous profile) changes to astrocyte subtypes (Fig 5B). When ATP is introduced, all distributions curves aggregate (Fig 5C). The effect of ATP suggests a minimization between the global differences in astrocyte populations. This minimization is reflected in the strongly overlapping distributions.

Next, we discuss mutual information. In spontaneous conditions, we find that the distributions for the astrocyte polygonal and stellate astrocytes are similar (and lower than reactive). These results suggests that spontaneously polygonal and stellate astrocyte behave more independently than reactive astrocytes (Fig 5A). When LATB is introduced, all mutual information curves are shifted higher with reactive

astrocytes retaining larger values while polygonal and stellate astrocyte pairs are similar (Fig 5B). Interestingly, this result indicates that a breakdown in the cytoskeleton causes uniformity in local behavior in astrocyte interactions (i.e. higher values of mutual information reflect less independence). When ATP is introduced, stellate astrocytes respond the most strongly (Fig 5C). Stellate astrocytes become strongly independent in terms of their local behavior. While stellate astrocytes respond the most strongly, all astrocyte subtypes become more independent (lower mutual information) when exposed to ATP.

Partitioned entropy highlights temporally local dynamics

We look at the partition entropy ratios for astrocytes in networks. Unlike with cross correlation and mutual information, partitioned entropy is a method for analyzing the dynamics of individual traces themselves (i.e. it is not a pairwise analysis method). As a dynamical measure, it provides more ability for understanding information dynamics than reporting entropy values alone. Partitioned entropy ratios are calculated by finding the average partitioned entropy across some time window (in this paper we chose to start at $\tau=10$ and end at $\tau=150$, see Supplement for details). Values of partitioned entropy closer to 1 are classified as chaotic whereas values closer to 0.5 are deemed limit cycles (e.g. sinusoidal oscillations). Classifying astrocytes in this way is beyond the scope of this work, but it is useful for further distinguishing dynamical profiles of the subtypes.

We find that spontaneously, astrocytes retain similar individual characteristics, as demonstrated in Fig 5D. This result is surprising given the numerous reported physiological differences in these subtypes. Coupled with some similarities across subtypes in the pairwise interactions results, we argue that, in spontaneous conditions, when astrocytes signal it is similar. This result suggests a universal characteristic to spontaneous astrocyte calcium events. LATB, comparable to the distinct effects in pairwise interactions, causes reactive astrocyte to behave more sinusoidally (Fig 5E). Stellate astrocytes respond with higher partitioned entropy ratios. Lastly, where LATB induces the strongest separation in cross-correlation distributions, ATP seems to induce a comparable outsized effect in the partitioned entropy curves shown in Fig 5F. The different perspective (focusing solely on the individual embedded dynamics) provided by partitioned entropy complements the results mentioned above in ascertaining the nuanced differences in astrocyte calcium signaling.

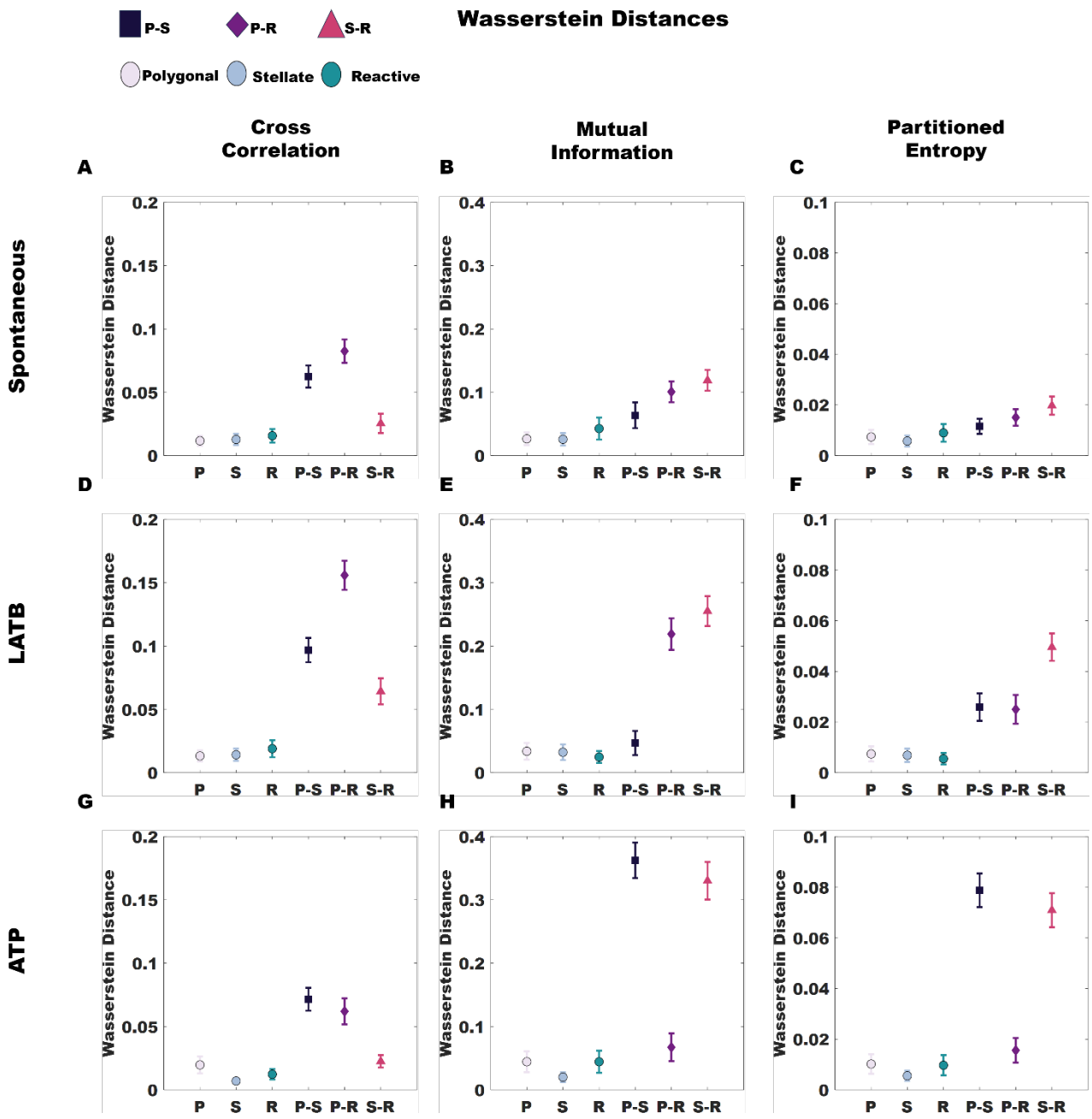

Fig 6: Wasserstein distances for the three classes of distributions shown in Fig 5. Astrocytes types are grouped; three pairs exist as highlighted by the dark (polygonal-stellate), purple (polygonal-reactive), and pink (stellate-reactive). We contrast these groups against the natural variance within the individual subtype distributions. We find the Wasserstein distances for: spontaneous (A) cross correlation (B) mutual information, and (C) partitioned entropy distributions, LATB exposed (D) cross correlation (E) mutual information, and (F) partitioned entropy distributions, and ATP induced (G) cross correlation (H) mutual information, and (I) partitioned entropy distribution. Results are bootstrapped.

Wasserstein distances enhance interpretability of comparisons

We use the Wasserstein distance (using its L1 norm definition, Wasserstein-1) to measure the differences in distributions shown in Fig 5. Wasserstein-1 quantifies the minimum distance needed to shift all points in a distribution to match another distribution. The Wasserstein distance considers the individual values used to generate the histograms in Fig 5., and is independent of the choice of bin. We can measure a

Wasserstein distance not only to compare distributions, but also to characterize a single distribution by using bootstrapping. Bootstrapping was performed for all Wasserstein-1 calculations with a sample size of 100 and 10,000 iterations. We can calculate Wasserstein distances for all metrics, cross correlation, mutual information, and partitioned entropy with this approach.

Under spontaneous conditions, polygonal cross correlation values are the most distinct (Fig 6A). Using symbolization, we find that the differences between stellate and reactive astrocytes (S-R) become most apparent for mutual information (Fig 6B) and partitioned entropy (Fig 6C). Thus, we conclude that on a global interaction perspective, polygonal dynamics behave the most uniquely; on a local level (using the embedded symbol states to understand dynamics), we find that spontaneously stellate astrocytes have a unique dynamical profile relative to the reactive subtype. The ability of information theory to tease out this result is significant. Both stellate and reactive astrocytes possess branches[82]. The process formation could have implicated such processes in the similarities seen in their cross-correlation distributions (S-R of Fig 6A).

Relative to spontaneous conditions, LATB increases the differences in the distributions for cross-correlation (Fig 6D), mutual information (Fig 6E), and partitioned entropy (Fig 6F). Where again, we see that polygonal astrocytes on a global level are the most distinct relative to stellate and reactive astrocytes (Fig 6D), but we find that in the mutual information distributions, P-R and S-R, reactive astrocytes separate the most strongly. This suggests reactive astrocytes are more susceptible to cytoskeletal perturbation, limiting pairwise signal propagation. Importantly, the high Wasserstein distances in Figs. 6D and 6E distinguish polygonal and reactive (P-R) astrocytes despite the similarities in AQP4 expression. The strongest separation in terms of individual trace dynamics is seen in S-R (Fig 6F), suggesting a strong difference in effect when healthy (stellate) versus unhealthy (reactive) astrocytes are exposed to LATB.

Lastly, it is interesting that the highest reported Wasserstein distances for mutual information (Fig 6H) and partitioned entropy (Fig 6I) are found under exposure to ATP. The lowest differences are attributed to the cross-correlation (Fig 6G). Outside of physiological comparisons, this highlights the importance of the diverse set of information theoretic tools used for understanding astrocyte signal dynamics. In contrast to the effect of LATB, ATP appears to cause the entire network to become excited (i.e. hyper-active), consistent with its known role as a key gliotransmitter. The lowest Wasserstein differences (across all conditions) are reported for P-R. Indeed, this result indicates that stellate astrocytes are the most susceptible to ATP intervention (P-S and S-R in Figs. 6H and 6G) whereas polygonal astrocytes share the unhealthy characteristics of reactive astrocytes (P-R).

Discussion

Collective astrocyte dynamics are rich in information distinct from neurons and previously overlooked. Starting from filtering out inactive traces with the non-biased Hurst exponent, we employed cross correlation, mutual information, and partitioned entropy to ascertain the dynamical properties of collections of maturing (polygonal), healthy (stellate), and injured (reactive) astrocytes. This behavior characterization extends to these astrocyte networks defined by distinct states (subtypes defined by differences e.g., in molecular expression, morphology) and when gliotransmitters or biomechanics (LATB) of the system is altered. Interestingly, this focus on information differences allowed us to demonstrate uniformity in the speed of information transport across astrocyte subtype and extracellular environment (ATP/LATB). Our analysis on these astrocyte networks handles the complex spatiotemporal patterns present in these data. Not merely regarding the calcium signaling of astrocytes as an adaptive mechanism, our work argues that the spatiotemporal patterns embedded in these networks are active. That

478 these patterns themselves are sources of dense information rivaling neuronal networks. The
479 spatiotemporal patterning of spontaneous astrocytes is shown in the Supplement.

480 A principal finding of this work is the corroboration of astrocyte signaling (Ca2+ waves) speed using
481 information theoretic methods. Using cross correlation and mutual information on astrocyte traces,
482 aggregating traces from independent image sequences, we find an invariance of the speed of information
483 transport. We discovered that for all conditions investigated, the speed of information transport is
484 approximately 25-40 μm/sec, consistent with the speed of Ca^{2+} waves measured directly in prior studies
485 [49,83,84]. These findings are independent of astrocyte subtype and chemical milieu, which strongly indicates
486 that Ca^{2+} waves are the primary mechanism of astrocyte-to-astrocyte information exchange, i.e. Ca^{2+}
487 dynamics is a dominant form of communication in astrocyte networks for all states and environmental
488 conditions investigated despite differences in molecular expression, information processing, and the
489 biochemical cell-cell coupling machinery (AQP4, Cx43). Given that we will subsequently discuss the
490 differences in information dynamics, this result is even more startingly. Confirmation of the speed of
491 information transport with previously reported values lends confidence to using these methods for
492 understanding astrocyte signals.

493 We preface subsequent interpretations of our results with subtle distinctions between the competing
494 pairwise information theoretic concepts in this work. Correlation (of which cross is the most appropriate
495 for astrocyte signals; see Supplement for more details) deals with the specific similarities of mean field
496 fluctuations of the traces. One way to understand this subtle concept is that pairwise correlation values
497 relate to the absolute coarse-grained differences between points in a time series. Accounting for the time
498 lag to maximize correlation, in the context of astrocyte signals, it describes how similar the calcium
499 events look; the average area overlap of all calcium events. Mutual information, supported by
500 symbolization, is more focused and able to provide more local descriptions of how symbol state
501 influences across time series[85]Both are important, and our results, such as the marked separation between
502 cross-correlation LATB distributions, indicate that both provide a holistic ability to compare astrocyte
503 dynamics. Indeed, an externality of these results, including the use of partitioned entropy for comparative
504 analysis, is a demonstration of the varied insights that are gained by using this complete set of
505 information theoretic tools.

506 Importantly, polygonal astrocytes in control conditions (spontaneous), which have been regarded as
507 quiescent,[19] exhibit information processing; in other words, polygonal cells are not inactive cells and
508 have complex signaling patterns. The difference between these polygonal cells, and stellate and reactive
509 astrocytes at first lies in the global correlation structure amongst polygonal astrocytes. As shown in Figs
510 6A,6D,6G, polygonal cells are the most distinct with higher cross correlation values than stellate and
511 reactive astrocytes. As correlation is a global averaging of time values, this suggests that the mean field
512 behavior of polygonal cells is more coupled than those of stellate and reactive astrocytes. In other words,
513 polygonal astrocytes broadly have more global network synchrony. These insights are counterintuitive as
514 the higher expression of the astrocyte markers regulating cell-cell coupling, AQP4 and Cx43, seen in
515 stellate and reactive astrocytes (Fig 1) suggest that these cells would couple more closely in their
516 information processing. One possible explanation is that the lower expression of coupling proteins limits
517 the signal propagation to fewer polygonal neighbors and thus, paradoxically, these polygonal networks
518 are globally more aligned. Future studies will investigate this possibility.

519 Locally, we gain additional insights into stellate and reactive signaling dynamics using symbolization
520 which embeds the dynamics. We conclude that reactive astrocytes respond most strongly to cytoskeletal
521 perturbation (LATB) whereas stellate astrocytes react most strongly to gliotransmitter ATP. These results
522 are consistent with the role of the cytoskeleton and ATP in reactive and stellate astrocytes, respectively.

Reactive astrocytes must have a dynamic cytoskeleton as they migrate to form the glial scar, an adaptive function in response to injury or disease[35,86]. Stellate astrocytes communicate via more localized contacts, and ATP is suggested to be an important extracellular messenger for specifically stellate-like calcium waves[87,88].

Overall, our work shows that applying information theoretic tools to *in vitro* astrocyte networks lends insights into the collective action of astrocytes. Generally, our work has analyzed the complex spatiotemporal characteristics of polygonal, stellate, and reactive networks. We find that polygonal astrocytes are not quiescent, stellate astrocytes respond most significantly to ATP, and reactive astrocytes are most affected by LATB. Our study also provides a systematic baseline of three complementary astrocyte states and key perturbations supporting future studies of astrocyte network function in health and disease. The successful demonstration of our method across numerous astrocyte conditions and microenvironments suggests broad applicability and promise for these tools to study astrocyte dynamics.

Acknowledgments

The authors thank the University of Maryland Imaging Incubator Core Facility for providing and maintaining the systems used in collecting images for this work. This work was supported by US Air Force Office of Scientific Research Astro-COLL grant FA9550-21-1-0352.

We want to thank Dr Leonard Campanello for always being generous with his time and providing insightful guidance on the timescales of information. We additionally thank Prof Pratyush Tiwary for his comments and suggestions.

Software Availability

Software has been made available on GitHub at:
https://github.com/losertlab/Astrocyte_CollectiveNetworkInformation

1. Bellot-Saez, A., Kékesi, O., Morley, J. W. & Buskila, Y. Astrocytic modulation of neuronal excitability through K+ spatial buffering. *Neuroscience & Biobehavioral Reviews* **77**, 87–97 (2017).
2. Mahmoud, S., Gharagozloo, M., Simard, C. & Gris, D. Astrocytes Maintain Glutamate Homeostasis in the CNS by Controlling the Balance between Glutamate Uptake and Release. *Cells* **8**, 184 (2019).
3. Mola, M. G. *et al.* Cell Volume Regulation Mechanisms in Differentiated Astrocytes. *Cell Physiol Biochem* **55**, 196–212 (2021).
4. Bélanger, M., Allaman, I. & Magistretti, P. J. Brain Energy Metabolism: Focus on Astrocyte-Neuron Metabolic Cooperation. *Cell Metabolism* **14**, 724–738 (2011).

5. Verkhratsky, A. & Nedergaard, M. Physiology of Astroglia. *Physiological Reviews* **98**, 239–389 (2018).
6. Benfenati, V. & Ferroni, S. Water transport between CNS compartments: functional and molecular interactions between aquaporins and ion channels. *Neuroscience* **168**, 926–940 (2010).
7. Koch, C. & Segev, I. The role of single neurons in information processing. *Nature Neuroscience* **3**, 1171–1177 (2000).
8. Luo, L. *et al.* Ten years of Nature Reviews Neuroscience: insights from the highly cited. *Nature Reviews Neuroscience* **11**, 718–726 (2010).
9. Krogh, A. What are artificial neural networks? *Nature Biotechnology* **26**, 195–197 (2008).
10. Bassett, D. S. & Gazzaniga, M. S. Understanding complexity in the human brain. *Trends Cogn Sci* **15**, 200–209 (2011).
11. Bassett, D. S. & Bullmore, E. Small-world brain networks. *Neuroscientist* **12**, 512–523 (2006).
12. Bassett, D. S. & Sporns, O. Network neuroscience. *Nature Neuroscience* **20**, 353–364 (2017).
13. Mederos, S., González-Arias, C. & Perea, G. Astrocyte–Neuron Networks: A Multilane Highway of Signaling for Homeostatic Brain Function. *Frontiers in Synaptic Neuroscience* **10**, (2018).
14. Giaume, C., Koulakoff, A., Roux, L., Holcman, D. & Rouach, N. Astroglial networks: a step further in neuroglial and gliovascular interactions. *Nature Reviews Neuroscience* **11**, 87–99 (2010).
15. Scemes, E. & Giaume, C. Astrocyte calcium waves: what they are and what they do. *Glia* **54**, 716–725 (2006).
16. Semyanov, A., Henneberger, C. & Agarwal, A. Making sense of astrocytic calcium signals — from acquisition to interpretation. *Nature Reviews Neuroscience* **21**, 551–564 (2020).

583 17. Wang, Y. *et al.* Accurate quantification of astrocyte and neurotransmitter fluorescence
584 dynamics for single-cell and population-level physiology. *Nat Neurosci* **22**, 1936–1944
585 (2019).
586 18. Lia, A. *et al.* Calcium Signals in Astrocyte Microdomains, a Decade of Great Advances.
587 *Frontiers in Cellular Neuroscience* **15**, (2021).
588 19. Wolfes, A. C. *et al.* A novel method for culturing stellate astrocytes reveals spatially distinct
589 Ca2+ signaling and vesicle recycling in astrocytic processes. *J Gen Physiol* **149**, 149–170
590 (2017).
591 20. Agarwal, A. *et al.* Transient Opening of the Mitochondrial Permeability Transition Pore
592 Induces Microdomain Calcium Transients in Astrocyte Processes. *Neuron* **93**, 587-605.e7
593 (2017).
594 21. Lagos-Cabré, R., Burgos-Bravo, F., Avalos, A. M. & Leyton, L. Connexins in Astrocyte
595 Migration. *Frontiers in Pharmacology* **10**, (2020).
596 22. Szu, J. I. & Binder, D. K. The Role of Astrocytic Aquaporin-4 in Synaptic Plasticity and
597 Learning and Memory. *Frontiers in Integrative Neuroscience* **10**, (2016).
598 23. Bortolami, A. & Sesti, F. Ion channels in neurodevelopment: lessons from the Integrin-
599 KCNB1 channel complex. *Neural Regeneration Research* **18**, (2023).
600 24. Nagelhus, E. A. & Ottersen, O. P. Physiological Roles of Aquaporin-4 in Brain. *Physiological*
601 *Reviews* **93**, 1543–1562 (2013).
602 25. Ohno, Y., Kunisawa, N. & Shimizu, S. Emerging Roles of Astrocyte Kir4.1 Channels in the
603 Pathogenesis and Treatment of Brain Diseases. *International Journal of Molecular Sciences*
604 **22**, (2021).
605 26. Benfenati, V. *et al.* An aquaporin-4/transient receptor potential vanilloid 4 (AQP4/TRPV4)
606 complex is essential for cell-volume control in astrocytes. *Proceedings of the National*
607 *Academy of Sciences* **108**, 2563–2568 (2011).

608 27. Fan, Y.-Y. & Huo, J. A1/A2 astrocytes in central nervous system injuries and diseases:
609 Angels or devils? *Neurochemistry International* **148**, 105080 (2021).
610 28. Ben Haim, L. & Escartin, C. Astrocytes and neuropsychiatric symptoms in
611 neurodegenerative diseases: Exploring the missing links. *Current Opinion in Neurobiology*
612 **72**, 63–71 (2022).
613 29. Homkajorn, B., Sims, N. R. & Muyderman, H. Connexin 43 regulates astrocytic migration
614 and proliferation in response to injury. *Neuroscience Letters* **486**, 197–201 (2010).
615 30. Rodnight, R. B. & Gottfried, C. Morphological plasticity of rodent astroglia. *Journal of*
616 *Neurochemistry* **124**, 263–275 (2013).
617 31. Gradisnik, L. & Velnar, T. Astrocytes in the central nervous system and their functions in
618 health and disease: A review. *World J Clin Cases* **11**, 3385–3394 (2023).
619 32. Liddelow, S. A. & Barres, B. A. Reactive Astrocytes: Production, Function, and Therapeutic
620 Potential. *Immunity* **46**, 957–967 (2017).
621 33. Escartin, C. *et al.* Reactive astrocyte nomenclature, definitions, and future directions. *Nature*
622 *Neuroscience* **24**, 312–325 (2021).
623 34. Lawal, O., Ulloa Severino, F. P. & Eroglu, C. The role of astrocyte structural plasticity in
624 regulating neural circuit function and behavior. *Glia* **70**, 1467–1483 (2022).
625 35. Zhou, B., Zuo, Y.-X. & Jiang, R.-T. Astrocyte morphology: Diversity, plasticity, and role in
626 neurological diseases. *CNS Neuroscience & Therapeutics* **25**, 665–673 (2019).
627 36. Baldwin, K. T., Murai, K. K. & Khakh, B. S. Astrocyte morphology. *Trends Cell Biol* S0962-
628 8924(23)00204–0 (2023) doi:10.1016/j.tcb.2023.09.006.
629 37. Nicchia, G. P. *et al.* Aquaporin-4 orthogonal arrays of particles from a physiological and
630 pathophysiological point of view. *Wiley Interdisciplinary Reviews: Membrane Transport and*
631 *Signaling* **2**, 143–154 (2013).

632 38. Mola, M. G. *et al.* The speed of swelling kinetics modulates cell volume regulation and
633 calcium signaling in astrocytes: A different point of view on the role of aquaporins. *Glia* **64**,
634 139–154 (2016).
635 39. Posati, T. *et al.* A Nanoscale Interface Promoting Molecular and Functional Differentiation of
636 Neural Cells. *Scientific Reports* **6**, 31226 (2016).
637 40. Saracino, E. *et al.* Extracellular Recording Systems: A Glial-Silicon Nanowire Electrode
638 Junction Enabling Differentiation and Noninvasive Recording of Slow Oscillations from
639 Primary Astrocytes (Adv. Biosys. 4/2020). *Advanced Biosystems* **4**, 2070044 (2020).
640 41. O'Neill, K. M. *et al.* Decoding Natural Astrocyte Rhythms: Dynamic Actin Waves Result from
641 Environmental Sensing by Primary Rodent Astrocytes. *Adv Biol (Weinh)* e2200269 (2023)
642 doi:10.1002/adbi.202200269.
643 42. Giralt, A., Coura, R. & Girault, J.-A. Pyk2 is essential for astrocytes mobility following brain
644 lesion. *Glia* **64**, 620–634 (2016).
645 43. Mitsushima, M., Takahashi, H., Shishido, T., Ueda, K. & Kioka, N. Abl kinase interacts with
646 and phosphorylates vinexin. *FEBS Letters* **580**, 4288–4295 (2006).
647 44. Tomás, M. *et al.* Protective effects of lysophosphatidic acid (LPA) on chronic ethanol-
648 induced injuries to the cytoskeleton and on glucose uptake in rat astrocytes. *Journal of*
649 *Neurochemistry* **87**, 220–229 (2003).
650 45. Bowser, D. N. & Khakh, B. S. ATP Excites Interneurons and Astrocytes to Increase Synaptic
651 Inhibition in Neuronal Networks. *J. Neurosci.* **24**, 8606 (2004).
652 46. Guthrie, P. B. *et al.* ATP Released from Astrocytes Mediates Glial Calcium Waves. *J.*
653 *Neurosci.* **19**, 520 (1999).
654 47. Zimmermann, H. Signalling via ATP in the nervous system. *Trends in Neurosciences* **17**,
655 420–426 (1994).
656 48. Burnstock, G. Cotransmission. *Current Opinion in Pharmacology* **4**, 47–52 (2004).

657 49. Giaume, C. & Venance, L. Intercellular calcium signaling and gap junctional communication
658 in astrocytes. *Glia* **24**, 50–64 (1998).
659 50. Yu, P., Wang, H., Katagiri, Y. & Geller, H. M. An In Vitro Model of Reactive Astrogliosis and
660 Its Effect on Neuronal Growth. *Methods Mol Biol* **814**, 327–340 (2012).
661 51. Ahmed, Z. S. O., Hussein, S., Ghandour, R. A., Azouz, A. A. & El-Sakhawy, M. A.
662 Evaluation of the effect of methotrexate on the hippocampus, cerebellum, liver, and kidneys
663 of adult male albino rat: Histopathological, immunohistochemical and biochemical studies.
664 *Acta Histochemica* **123**, 151682 (2021).
665 52. Bramanti, V., Tomassoni, D., Avitabile, M., Amenta, F. & Avola, R. Biomarkers of glial cell
666 proliferation and differentiation in culture. *FBS* **2**, 558–570 (2010).
667 53. Cibelli, A. *et al.* Aquaporin-4 and transient receptor potential vanilloid 4 balance in early
668 postnatal neurodevelopment. *Glia* **72**, 938–959 (2024).
669 54. Berger, J. V. *et al.* Opposite regulation of metabotropic glutamate receptor 3 and
670 metabotropic glutamate receptor 5 by inflammatory stimuli in cultured microglia and
671 astrocytes. *Neuroscience* **205**, 29–38 (2012).
672 55. Song, C., Zhang, Y. & Dong, Y. Acute and subacute IL-1β administrations differentially
673 modulate neuroimmune and neurotrophic systems: possible implications for neuroprotection
674 and neurodegeneration. *Journal of Neuroinflammation* **10**, 826 (2013).
675 56. Tilleux, S. & Hermans, E. Neuroinflammation and regulation of glial glutamate uptake in
676 neurological disorders. *Journal of Neuroscience Research* **85**, 2059–2070 (2007).
677 57. Tilleux, S., Berger, J. & Hermans, E. Induction of astrogliosis by activated microglia is
678 associated with a down-regulation of metabotropic glutamate receptor 5. *Journal of*
679 *Neuroimmunology* **189**, 23–30 (2007).
680 58. Sullivan, S. M. *et al.* Cytoskeletal Anchoring of GLAST Determines Susceptibility to Brain
681 Damage: AN IDENTIFIED ROLE FOR GFAP *. *Journal of Biological Chemistry* **282**, 29414–
682 29423 (2007).

683 59. Toops, K. A., Hagemann, T. L., Messing, A. & Nickells, R. W. The effect of glial fibrillary
684 acidic protein expression on neurite outgrowth from retinal explants in a permissive
685 environment. *BMC Research Notes* **5**, 693 (2012).
686 60. Chalfoun, J. *et al.* FogBank: a single cell segmentation across multiple cell lines and image
687 modalities. *BMC Bioinformatics* **15**, 431 (2014).
688 61. Giovannucci, A. *et al.* CaImAn an open source tool for scalable calcium imaging data
689 analysis. *eLife* **8**, e38173 (2019).
690 62. Bowen, Z., Winkowski, D. E., Seshadri, S., Plenz, D. & Kanold, P. O. Neuronal Avalanches
691 in Input and Associative Layers of Auditory Cortex. *Frontiers in Systems Neuroscience* **13**,
692 (2019).
693 63. Simonsen, I., Hansen, A. & Nes, O. M. Determination of the Hurst exponent by use of
694 wavelet transforms. *Phys. Rev. E* **58**, 2779–2787 (1998).
695 64. Generalized Hurst exponent.
696 https://www.mathworks.com/matlabcentral/fileexchange/30076-generalized-hurst-exponent
697 (2023).
698 65. Averbeck, B. B., Latham, P. E. & Pouget, A. Neural correlations, population coding and
699 computation. *Nat Rev Neurosci* **7**, 358–366 (2006).
700 66. Panzeri, S., Schultz, S. R., Treves, A. & Rolls, E. T. Correlations and the encoding of
701 information in the nervous system. *Proc Biol Sci* **266**, 1001–1012 (1999).
702 67. Cohen, M. R. & Kohn, A. Measuring and interpreting neuronal correlations. *Nat Neurosci* **14**,
703 811–819 (2011).
704 68. Kohn, A., Coen-Cagli, R., Kanitscheider, I. & Pouget, A. Correlations and Neuronal
705 Population Information. *Annual Review of Neuroscience* **39**, 237–256 (2016).
706 69. Aguado, F., Espinosa-Parrilla, J. F., Carmona, M. A. & Soriano, E. Neuronal Activity
707 Regulates Correlated Network Properties of Spontaneous Calcium Transients in Astrocytes
708 In Situ. *J Neurosci* **22**, 9430–9444 (2002).

70. Daw, C. S., Finney, C. E. A. & Tracy, E. R. A review of symbolic analysis of experimental data. *Review of Scientific Instruments* **74**, 915–930 (2003).
71. Cao, Y., Tung, W., Gao, J. B., Protopopescu, V. A. & Hively, L. M. Detecting dynamical changes in time series using the permutation entropy. *Phys. Rev. E* **70**, 046217 (2004).
72. Shiozawa, K., Uemura, T. & Tokuda, I. T. Detecting the dynamical instability of complex time series via partitioned entropy. *Phys. Rev. E* **107**, 014207 (2023).
73. Lungarella, M., Pitti, A. & Kuniyoshi, Y. Information transfer at multiple scales. *Phys. Rev. E* **76**, 056117 (2007).
74. Schreiber, T. Measuring Information Transfer. *Phys. Rev. Lett.* **85**, 461–464 (2000).
75. Lehnertz, K. Ordinal methods for a characterization of evolving functional brain networks. *Chaos: An Interdisciplinary Journal of Nonlinear Science* **33**, 022101 (2023).
76. Staniek, M. & Lehnertz, K. Symbolic Transfer Entropy. *Phys. Rev. Lett.* **100**, 158101 (2008).
77. Staniek, M. & Lehnertz, K. Symbolic transfer entropy: inferring directionality in biosignals. **54**, 323–328 (2009).
78. STANIEK, M. & LEHNERTZ, K. PARAMETER SELECTION FOR PERMUTATION ENTROPY MEASUREMENTS. *Int. J. Bifurcation Chaos* **17**, 3729–3733 (2007).
79. Bandt, C. & Pompe, B. Permutation Entropy: A Natural Complexity Measure for Time Series. *Phys. Rev. Lett.* **88**, 174102 (2002).
80. Li, S., Xiao, Y., Zhou, D. & Cai, D. Causal inference in nonlinear systems: Granger causality versus time-delayed mutual information. *Phys. Rev. E* **97**, 052216 (2018).
81. Vastano, J. A. & Swinney, H. L. Information transport in spatiotemporal systems. *Phys. Rev. Lett.* **60**, 1773–1776 (1988).
82. Khakh, B. S. & Sofroniew, M. V. Diversity of astrocyte functions and phenotypes in neural circuits. *Nature Neuroscience* **18**, 942–952 (2015).

83. Glaum, S. R., Holzwarth, J. A. & Miller, R. J. Glutamate receptors activate Ca2+ mobilization and Ca2+ influx into astrocytes. *Proceedings of the National Academy of Sciences* **87**, 3454–3458 (1990).

84. Charles, A. C., Merrill, J. E., Dirksen, E. R. & Sandersont, M. J. Intercellular signaling in glial cells: Calcium waves and oscillations in response to mechanical stimulation and glutamate. *Neuron* **6**, 983–992 (1991).

85. Fraser, A. M. & Swinney, H. L. Independent coordinates for strange attractors from mutual information. *Phys. Rev. A* **33**, 1134–1140 (1986).

86. Schiweck, J., Eickholt, B. J. & Murk, K. Important Shapeshifter: Mechanisms Allowing Astrocytes to Respond to the Changing Nervous System During Development, Injury and Disease. *Frontiers in Cellular Neuroscience* **12**, (2018).

87. Li, S., Graham, E. S. & Unsworth, C. P. Extracellular ATP release predominantly mediates Ca2+ communication locally in highly organised, stellate-Like patterned networks of adult human astrocytes. *PLOS ONE* **18**, e0289350 (2023).

88. Takano, H. *et al.* Micropatterned Substrates: Approach to Probing Intercellular Communication Pathways. *Anal. Chem.* **74**, 4640–4646 (2002).